Distribution of subsurface residual stress as a function of wall thickness in stainless steel 316L LPBF structures

Cheng-Han Yu, Maximilian Sprengel, Jakob Schröder, Itziar Serrano-Munoz, Gunther Mohr, Alexander Evans, Arne Kromm, Ru Lin Peng, Thomas Kannengiesser, Giovanni Bruno, et al.

DISTRIBUTION OF SUBSURFACE RESIDUAL STRESS AS A FUNCTION OF WALL THICKNESS IN STAINLESS STEEL 316L LPBF STRUCTURES

Cheng-Han Yu[a,c], Maximilian Sprengel[b,c], Jakob Schröder[b], Itziar Serrano-Munoz[b], Gunther Mohr[b], Alexander Evans[b], Arne Kromm[b], Ru Lin Peng[a], Thomas Kannengiesser[b], Giovanni Bruno[b] and Johan Moverare[a]

[a] *Linköping University, Department of Management and Engineering, 58183 Linköping, Sweden*
[b] *Bundesanstalt für Materialforschung und -prüfung (BAM), Unter den Eichen 87, 12205 Berlin, Germany*
[c] *These authors contributed equally: Cheng-Han Yu, Maximilian Sprengel*

ABSTRACT

In this study, the surface and subsurface residual stress (RS) in thin-walled laser powder bed fused as-built stainless steel 316L was characterised using X-ray diffraction combined with electro-polishing layer removal method. The aim was to elucidate the influence of the wall thickness and surface roughness on the formation and magnitudes of surface and subsurface RS. For this purpose, rectangular specimen with three different wall thicknesses of 2, 5, and 9 mm were analysed. By electropolishing, RS depth profiles measurements were performed up to a depth of 200 μm. The results show a decrease of the surface RS in the thinner specimens. The depth profiles display a steep gradient of the subsurface tensile RS, whereby the location of the maximum subsurface RS is dependent on the wall thickness. The thinnest specimen exhibits the lowest maximum tensile RS and a tendency to zero stress at shallower depth. The shape of the RS depth profiles is observed to be related to the surface roughness, where the higher surface roughness leads to a milder increasing gradient of the subsurface RS.

Keywords: residual stress; X-ray diffraction; laser powder bed fusion stainless steel; surface roughness

1. Introduction

Additive Manufacturing (AM) has been in the focus of industry and research in the past decade as it pushes the boundaries of design and functionalization of components. In fact, AM processes such as Laser Powder Bed Fusion (LPBF) offer the promise of exceptional weight-savings of designs combined with comparable mechanical properties to conventionally processed material. However, the rapid cooling in the LPBF process lead to residual stress (RS) in the part after production [1]. These RS can deteriorate the mechanical properties, especially the fatigue resistance [2]. The number of studies which have reported the influence of the geometry on the subsurface RS distribution remains scarce. Baylerlein et al. observed a constant distribution of the RS with increasing heights in LPBF IN718 specimens [3]. Ghasri- Khouzani et al. investigated the RS distribution and sample distortion in LPBF 316L disc-shape specimens with varying thicknesses and diameters [4] for components built horizontally. A clear trend of lower in-plane RS and higher geometrical distortion in the thinner specimens was found, which is in agreement with the observation of Mercelis et al. [5].

The surface and the bulk regions are different in terms of texture [6] and RS [7]. To characterise the depth resolved distribution of RS between the two regions, it is often necessary to use complementary methods. Multiple methods can be applied to determine the subsurface RS distribution, for instance, hole-drilling strain-gauge method [8], synchrotron X-ray diffraction [9], neutron diffraction [7], and neutron Bragg edge imaging [6]. However,

*Corresponding author: Cheng-Han Yu. cheng-han.yu@liu.se

considering the limited accessibility of the measurement methods by using large-scale facility [7], combining laboratory XRD with layer removal by electropolishing is a suitable and efficient approach to determine the RS distribution semi-destructively. The design freedom of LPBF components needs to be secured by fundamental understanding of the geometrical effects. Hence, the influence of the thickness on the RS formation at the subsurface (i.e., 200 µm depth) is investigated in this study. The surface and subsurface RS are determined by using X-ray diffraction (XRD) and electrolytic layer removal. For comparison purposes between the LPBF 316L specimens, the XRD measurements are complemented by surface roughness measurements. To maintain a single controlling variable in this study, all the specimens were printed within the same batch with the identical process parameters. The results show that the wall thickness influences both the surface and subsurface RS distribution and the magnitude of the maximum tensile RS.

2. Experiments & method

2.1 Sample Manufacturing

The rectangular specimens of AISI 316L austenitic stainless steel (Fe-17Cr-12Ni) were additively manufactured at BAM, Berlin, Germany, within the same building batch in a SLM Solutions 280HL (SLM Solutions Group AG, Germany) LPBF machine. The position of the as-built specimens on the build-plate is shown in Figure 1a. The scanning strategy applied was the meander stripe with 90˚ scanning rotation. The scanning vectors were aligned with the geometrical axes of the rectangular specimens, which are the longitudinal direction (LD) and the transverse direction (TD) directions in Figure 1b. The process parameters are given as follows; layer thickness of 50 µm, laser power of 275 W, scanning velocity of 700 mm/s, and hatch distance of 0.12 mm. The AISI 316L powder was produced by gas atomization (nitrogen) and the particle size distribution was D10 = 18 µm, D50 = 31 µm, and D90 = 56 µm. 40 mm (height) x 26 mm (width) rectangular specimens were built with three different thicknesses (t): 2 mm, 5 mm and 9 mm. The samples were built vertically; (building direction (BD)), i.e their longest dimension was 90° to the build plate. After manufacturing, the specimens were removed from the build plate by saw cutting.

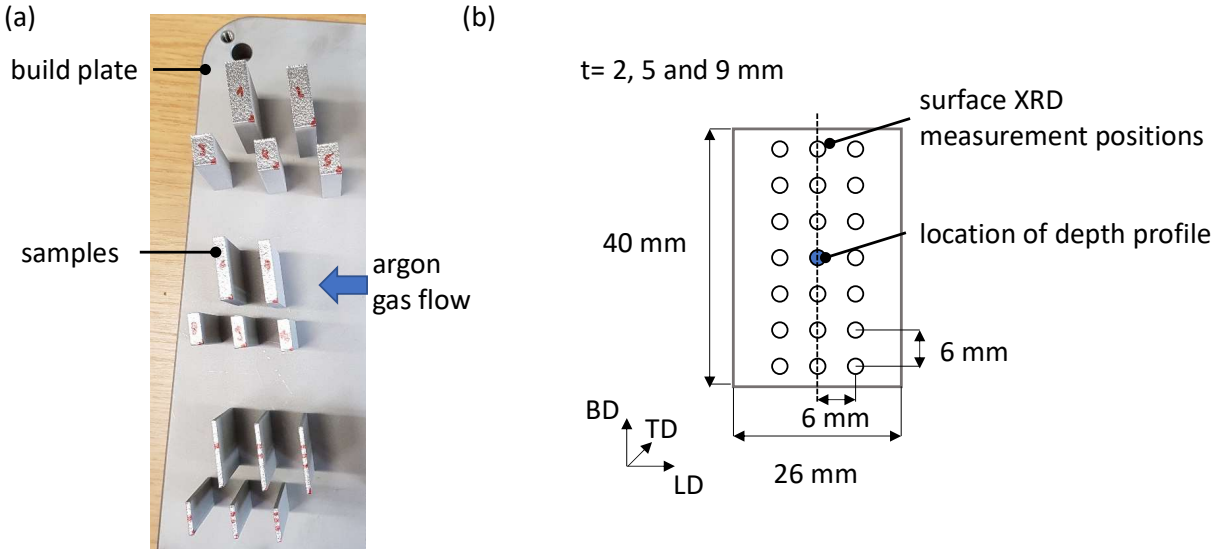

Figure 1. (a) The position of the as-built specimens on the built plate. (b) Schematic illustrations of the specimens. The open circles refer to the surface RS measurement locations, and the blue circle refers to the area for the subsurface RS depth profile measurement.

2.2 Residual Stress Determination

The surface and subsurface RS were determined on an Xstress G3 mobile diffractometer (StressTech Oy, Vaajakoski, Finland) using the $\sin^2\psi$-method. The parameters for the

acquisition of the diffraction peaks and the calculation of the RS are given in Table 1. The elastic constants E and ν were calculated with the software XEC using the Eshelby-Kröner model, the applicability of which to LPBF 316L was proven by Chen et al. [10]. The parameters were kept constant throughout the investigation. For the surface RS maps, a 3 x 7 measuring points matrix was applied at the centre of each specimen surface. The RS was determined along the BD. For the depth profiles, the RS in both the building direction (BD) and the LD were determined.

Table 1. Measurement parameters for the RS determination.

Current in mA	6.7	Young's modulus E (311) in GPa	184
Voltage in kV	30	Poisson's ratio ν (311)	0.294
Radiation	MnKa	Collimator diameter in mm	2
Reflection / 2θ in °	Fe – 311 / 152	Acquisition time in s	5
Ψ – angle range in°	-45 to 45 (19 steps)	Peak fitting	Pearson VII

2.3 Depth Profile of Subsurface Residual Stress Determination

Depth profiles of subsurface residual stress were obtained by a stepwise layer removal in the TD-direction (thickness). An electropolishing system Kristall 650 (ATM GmbH) was used to perform the layer removal. A voltage of 30 V was applied for a duration of 10 seconds. The electropolishing solution was composed of 550 ml of saturated saline solution (NaCl 359 g/l at room temperature), 150 ml of H_2O, 200 ml of ethylene glycol $C_2H_6O_2$ and 100 ml of ethanol C_2H_6O. The depth of the layer removal was measured using a dial indicator (Digimatic dial indicator ID-C series 543-471 B, Mitutoyo). Due to manual polishing, the step size of layer removal varies between 15 µm and 25 µm. The maximum depth of layer removal was 200 µm.

2.4 Surface Roughness Determination

The roughness of selected specimen surfaces (the area close to the blue circle in Figure 1b) was measured using MarSurf CM expert confocal microscope (NanoFocus AG, Oberhausen, Germany). The measurement parameters were identical for each specimen. The measurement position was 10 mm away from the sample's top and close to the position of the layer removal. The images were taken with a 20× magnification (objective 800XS). The roughness values Sa (arithmetic mean height), Sz (maximum height), Sv (maximum pit height) and Sp (maximum peak height) of a 2 × 2 mm^2 area were calculated using the software µsoft (NanoFocus AG, Oberhausen, Germany) according to ISO 4288.

3. Results

3.1 Surface Residual Stress

The surface σ_{BD} maps of the three specimens are shown in Figure 2. A higher surface RS is found for the 9 mm specimen, while a similar level of RS is observed in the 2 mm and the 5 mm specimens. A lower RS at the middle of the map is observed in all the specimens, while a larger RS difference (between the local minimum and the average surface RS) is found in the 2 mm specimen compared to the 5 mm specimen. Lower RS is found at the bottom of each specimen (approximately 2 mm from the cut surface), corresponding to the boundary condition of the free surface in the building direction resulting from removal from the baseplate.

3.2 Depth Profiles

The depth profiles of the RS, in BD and in LD, (TD-direction) are shown in Figure 3. The depth profile was measured at the centre of each specimen. A sharp increase of the RS in the

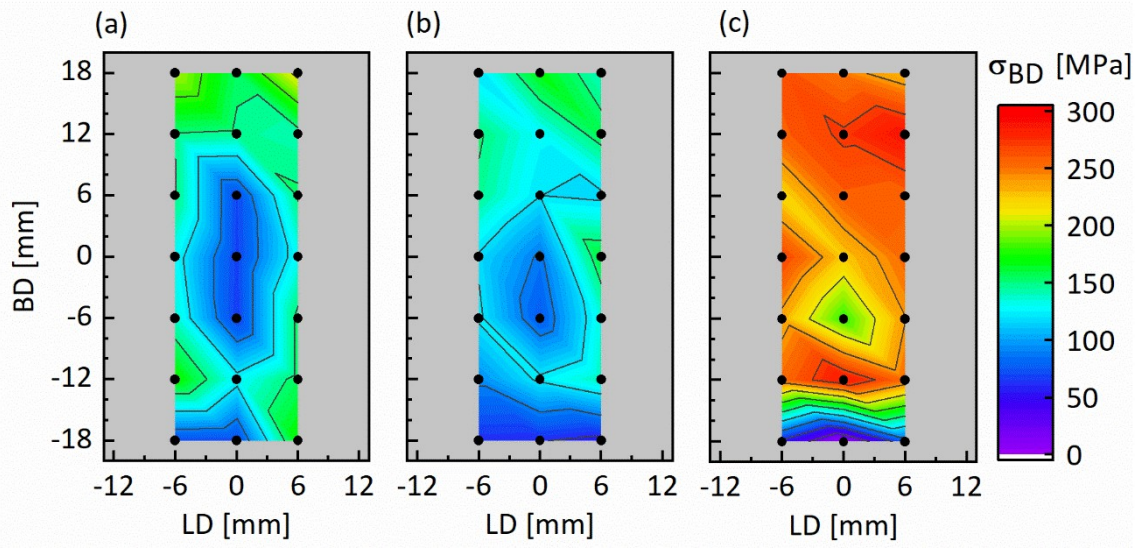

Figure 2. Surface σ_{BD} maps for the samples with different thicknesses. (a) Thickness of 2 mm. (b) Thickness of 5 mm. (c) Thickness of 9 mm.

BD is observed over the depth of 25 µm. The tendency found in all the three specimens after reaching the depth at around 25 µm varies significantly: the RS decreases continuously with the depth in the 2 mm specimen, while an increase of the RS is observed in the 5 mm and 9 mm thick specimens. The RS magnitudes in the BD are much higher in the 5 mm and the 9 mm specimens compared to the 2 mm specimen. Although different gradients of increasing RS are observed for the 5mm and 9mm specimens, the RS reaches a similar level of around 350 MPa at greater depth (around 100 µm). These values are around 80 % of the yield strength of LPBF 316L as reported in [11]. In general, the RS in the LD is lower than the RS in the BD. In addition, an abrupt increase of the RS in LD in the 5 mm and the 9 mm specimens to a level of about 200 MPa is observed in the range of 125 – 175 µm in depth (Figure 3b).

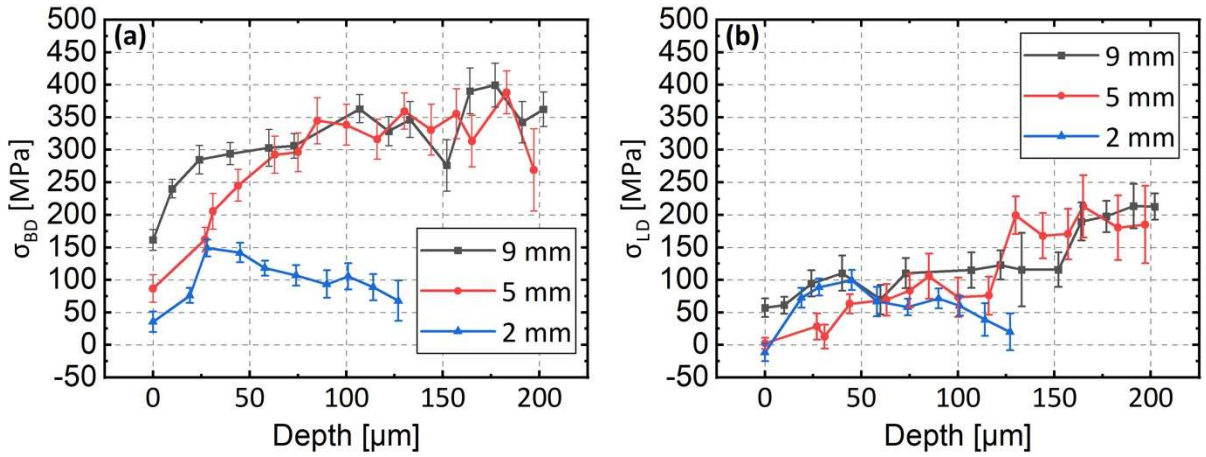

Figure 3. ***Depth profiles of RS in the thickness direction (TD) of the three specimens. (a) RS in BD. (b) RS in LD. Note that the 0 µm position in TD refers to the specimen surface, and the layer removal is along the TD.***

3.3 Surface Roughness

The surface roughness of each specimen is shown in Figure 4, and the roughness parameters are summarized in Table 2. The highest surface roughness is found for the 5 mm specimen, while similar surface roughness is observed for the 2 mm and the 9 mm specimens. In general, the topology of the surface roughness of all three specimens is constructed of stripe-like bulges and dot-like features. The dot-like features are semi-melted powder particles on the surface. The stripe-like bulges are expected to be the result of the layer-by-layer manufacturing process, although do not represent each individual layer. Horizontal bulges are clearly observed for the

2 mm and the 9 mm specimens. Surprisingly, the surface roughness morphology of the 5 mm specimen is significantly different. The corresponding roughness values are much higher (Sa =14.29 µm) compared to the 2 mm and the 9 mm specimens and the bulges are observed to be orientated vertically.

Table 2. Area roughness parameters of Sa, Sz, Sv and Sp for each specimen. Note that the unit is in µm.

Thickness	Sa	Sz	Sv	Sp
2mm	7.29	78.62	39.36	39.26
5mm	14.29	147.3	82.86	64.46
9mm	7.44	71.14	35.2	35.94

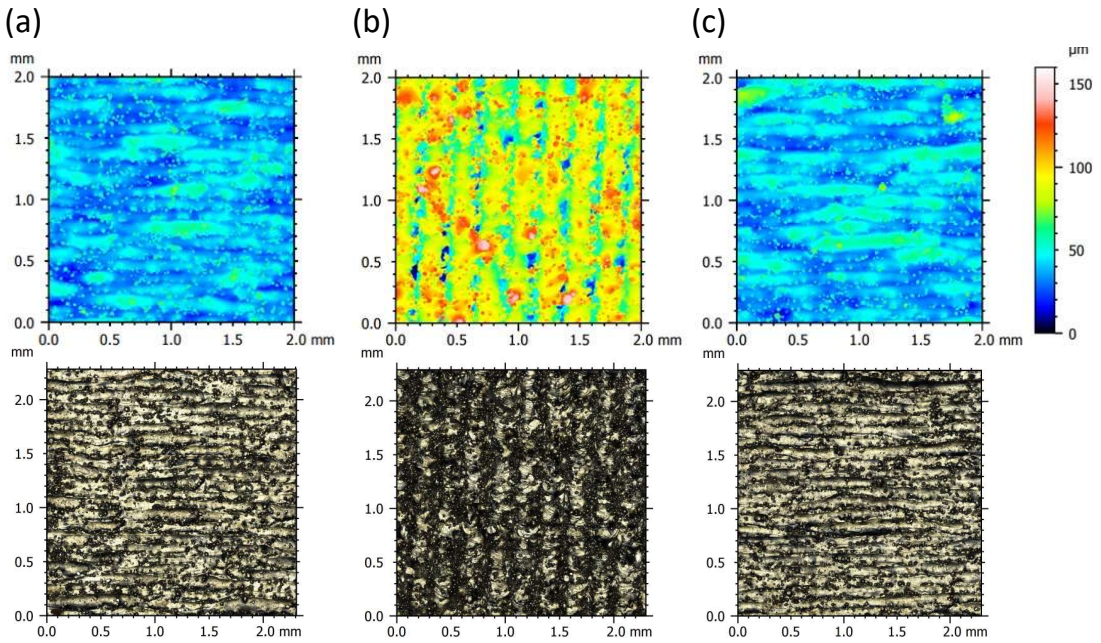

Figure 4. Surface roughness of (a) 2mm specimen, (b) 5mm specimen, and (c) 9mm. Note that the BD is along the vertical direction of each graph. The figures in the bottom row are the images from the confocal microscope.

4. Discussion

4.1 Surface Residual Stress

The surface RS of all specimens exhibit a local minimum at the central region of the specimens, see Figure 2. This distribution could result from the stress relaxation arising due to a geometrical distortion. Wu et al. observed the correlation between the RS relaxation and the geometrical distortion in a LPBF 316L specimen by using digital image correlation [12]. Although the sample geometry was different, a similar distribution of RS (lower RS in the central area at half the height of the specimen) was observed. The authors attributed this RS distribution to the geometrical distortion following the removal of the specimens from the build plate [12]. As high level and sharp gradient of RS are reported in LPBF steel [3], [13], [14], the specimen is assumed to distort during the removal from the build plate due to the relaxation of the high RS [4], [5]. From Ghasri-Khouzani et al., the level of distortion upon specimen removal is found to be geometry-dependent, whereby a larger distortion is expected in the thinner specimen [4]. This could explain the much lower surface RS of the 2 mm specimens compared to the 9 mm specimen. Multiple factors can influence the surface RS: for instance, the magnitude of the generated RS is affected by the different hatching length (due to the sample thickness), where higher RS has been reported for longer scan vector length [5], [12]. Therefore, the degree

of stress relaxation might also be different when removing the specimens from the build plate [15]. In addition, the surface roughness shown in Figure 4 could also lead to the variation of the surface RS since the penetration depth of the X-rays is low (5-10 µm) compared to the roughness induced by the semi-melted powder and the bulges. This effect was also observed in Mishurova et al. [9]. The mechanisms leading to the higher surface roughness observed for the 5 mm specimen remain unclear. A similar roughness was expected as the orientation of the surface and process parameters were identical. This question is left for future investigations, while the origin of the rotation of the bulges is currently unclear.

4.2 Subsurface Residual Stress

The variation of the RS depth profiles for the three specimen thicknesses are characterised by two features. The first is the significant difference is found between the 5 mm and 2 mm specimens in the BD. The second is both the differences and similarity between the 5mm and 9mm specimens. The position of the maximum tensile RS as shown in Figure 3 appears to be dependent on the thickness. This maximum RS is located at a depth of 25 µm for the 2 mm specimen and around 100 µm in the 5 mm specimen. A plateau in RS is reached for the 9mm specimen at a depth of 50 µm. This observation indicates that the location of the maximum RS in the 9 mm specimen is either reached (but stretches over a larger depth as reported by Serrano et al. [7]) or that it occurs at a greater depth such as observed in Busi et al.[6]. The decrease of the RS at the depth of 25 µm in the 2 mm specimen indicates a shallow tensile RS zone transitioning towards the compressive stress RS in the bulk of the specimen. Moreover, the lower magnitude of the subsurface tensile RS also infers that the lower compressive RS state can be expected in the bulk as the RS needs to balance over the part thickness. In contrast, the RS of the thicker specimens remains at a high level up to the measured depth of 200 µm. Although the surface RS in Figure 2 is different between the 9 mm and the 5 mm specimens, it is considered that above a critical threshold the RS subsurface depth profile would follow a similar trend. A similar observation was reported on the thin-walled Hastelloy-X LPBF specimens, although the alloy composition and manufacturing strategy are different [16]. Furthermore, it is assumed that the increased surface roughness directly influences the profile of the RS in the first layer removal steps. The gradient of RS between the surface and subsurface of the 5 mm is less steep compared to the 9 mm specimen (< 50 µm). A lower level of RS is expected in the semi-melted powder and bulges since these features cannot retain high stress. Hence, a lower surface RS averaged over the gauge volume is observed as a result. Moreover, as the number of steps of electropolishing are applied increases, the smoother the surface is expected to become, leading to higher constraint and therefore residual stress. However, further characterization effort is necessary to determine the correlation of subsurface RS profiles and surface roughness.

5. Conclusions

To investigate the effect of thickness on the surface and subsurface RS formation, AISI 316L specimens with thicknesses of 2 mm, 5 mm and 9 mm were built using LPBF. The following conclusions can be drawn:

1. In general, RS in the BD is higher than RS in LD for both surface and subsurface RS.
2. The analysis of the surface RS and subsurface RS yields diverging observations: the surface RS in the 2 mm and 5 mm specimens are similar, while a higher surface RS is found in the 9 mm specimen. However, similarly high RS values are observed in the subsurface for the 5 mm and 9 mm specimens compared to the 2 mm specimen.
3. The subsurface RS of the 5 mm specimen is assumed to be affected by the higher surface roughness compared to the two other specimen. This is thought to reduced RS gradient over the 0 - 50 µm depth. Otherwise, the depth profiles of the 5 mm and 9 mm specimens are broadly similar.
4. The analysis of the subsurface RS profiles reveals the link between the location of the subsurface maximum with the thickness; increasing the wall thickness shifts the peak tensile RS to greater depths.

6. Acknowledgements

This work has been funded by the BAM Focus Area Materials project AGIL. C.-H. Yu acknowledges the Swedish Governmental Innovation agency (Vinnova grant 2016-05175), the travel grant from the department of management and engineering (IEI) and faculty grant SFO-MATLiU#2009-00971 at Linköping University. We are thankful for the financial support and the cooperation with all partners.

References

[1] T. DebRoy *et al.*, "Additive manufacturing of metallic components – Process, structure and properties," *Prog. Mater. Sci.*, vol. 92, pp. 112–224, 2018, doi: 10.1016/j.pmatsci.2017.10.001.

[2] J. L. Bartlett and X. Li, "An overview of residual stresses in metal powder bed fusion," *Additive Manufacturing*. 2019, doi: 10.1016/j.addma.2019.02.020.

[3] F. Bayerlein, F. Bodensteiner, C. Zeller, M. Hofmann, and M. F. Zaeh, "Transient development of residual stresses in laser beam melting – A neutron diffraction study," *Addit. Manuf.*, vol. 24, no. October, pp. 587–594, 2018, doi: 10.1016/j.addma.2018.10.024.

[4] M. Ghasri-Khouzani *et al.*, "Experimental measurement of residual stress and distortion in additively manufactured stainless steel components with various dimensions," *Mater. Sci. Eng. A*, vol. 707, no. September, pp. 689–700, 2017, doi: 10.1016/j.msea.2017.09.108.

[5] P. Mercelis and J. P. Kruth, "Residual stresses in selective laser sintering and selective laser melting," *Rapid Prototyp. J.*, vol. 12, no. 5, pp. 254–265, 2006, doi: 10.1108/13552540610707013.

[6] M. Busi *et al.*, "Nondestructive characterization of laser powder bed fusion parts with neutron Bragg edge imaging," *Addit. Manuf.*, 2021, doi: 10.1016/j.addma.2021.101848.

[7] I. Serrano-Munoz *et al.*, "The Importance of Subsurface Residual Stress in Laser Powder Bed Fusion IN718," *Adv. Eng. Mater.*, vol. 2100895, pp. 1–7, 2021, doi: 10.1002/adem.202100895.

[8] R. Barros *et al.*, "Laser powder bed fusion of inconel 718: Residual stress analysis before and after heat treatment," *Metals (Basel).*, 2019, doi: 10.3390/met9121290.

[9] T. Mishurova, K. Artzt, J. Haubrich, G. Requena, and G. Bruno, "Exploring the correlation between subsurface residual stresses and manufacturing parameters in laser powder bed fused ti-6al-4v," *Metals (Basel).*, vol. 9, no. 2, 2019, doi: 10.3390/met9020261.

[10] W. Chen *et al.*, "Microscale residual stresses in additively manufactured stainless steel," *Nat. Commun.*, 2019, doi: 10.1038/s41467-019-12265-8.

[11] T. Ronneberg, C. M. Davies, and P. A. Hooper, "Revealing relationships between porosity, microstructure and mechanical properties of laser powder bed fusion 316L stainless steel through heat treatment," *Mater. Des.*, 2020, doi: 10.1016/j.matdes.2020.108481.

[12] A. S. Wu, D. W. Brown, M. Kumar, G. F. Gallegos, and W. E. King, "An Experimental Investigation into Additive Manufacturing-Induced Residual Stresses in 316L Stainless Steel," *Metall. Mater. Trans. A Phys. Metall. Mater. Sci.*, vol. 45, no. 13, pp. 6260–6270, 2014, doi: 10.1007/s11661-014-2549-x.

[13] R. J. Williams, F. Vecchiato, J. Kelleher, M. R. Wenman, P. A. Hooper, and C. M. Davies, "Effects of heat treatment on residual stresses in the laser powder bed fusion of 316L stainless steel: Finite element predictions and neutron diffraction measurements," *J. Manuf. Process.*, vol. 57, no. June, pp. 641–653, 2020, doi: 10.1016/j.jmapro.2020.07.023.

[14] A. Ulbricht *et al.*, "Separation of the formation mechanisms of residual stresses in lpbf 316l," *Metals (Basel).*, vol. 10, no. 9, pp. 1–15, 2020, doi: 10.3390/met10091234.

[15] T. Thiede *et al.*, "Residual stress in selective laser melted inconel 718: Influence of the removal from base plate and deposition hatch length," *Mater. Perform. Charact.*, 2018, doi: 10.1520/MPC20170119.

[16] C. H. Yu *et al.*, "Thin-wall effects and anisotropic deformation mechanisms of an additively manufactured Ni-based superalloy," *Addit. Manuf.*, vol. 36, p. 101672, 2020, doi: 10.1016/j.addma.2020.101672.